Multilinked Multirotor with Internal Communication System for Multiple Objects Transportation based on Form Optimization Control

Tomoki Anzai[1], Moju Zhao[1], Xiangyu Chen[1], Fan Shi[1], Koji Kawasaki[1], Kei Okada[1], Masayuki Inaba[1]

***Abstract*— In this paper, we show the achievement of a transformable aerial robot with internal communication system for multiple objects transportation. As it is not easy to make the endurance of an aerial robot longer, we focus on a way that aerial robot transports multiple objects at the same time to improve the efficiency of transportation. However, for conventional aerial robots, multiple objects transportation is difficult because the CoG position changes when the number of objects the aerial robot grasp changes, resulting in the instability of the flight. Therefore, to solve this problem, we focus on multirotor with two-dimensional multilinks in our previous work which possesses the ability to modify the position of CoG actively and can keep the flight stable. Moreover, we investigate a novel hardware structure of multilinks to extend the number of links. We explain the hardware platform including the structure of link module and internal communication system. We then propose a method to find the optimal form for the multilinks based on the flight stability. Finally, we present the experimental result which includes aerial transformation and multiple objects transportation.**

I. INTRODUCTION

Recently, aerial robots have attracted a lot of attention and have been studied actively due to their high mobility in three-dimensional environments[1]. While there are many application of aerial robots, such as surveillance[2], rescue[3], object manipulation and transportation by aerial robots has become an active area of research[4][5][6][7][8][9]. However, there are still some problems to solve about aerial object transportation. In particular, the endurance of aerial robots is a significant problem. To make the endurance longer, putting bigger batteries can be considered as a way, but the endurance does not scale linearly with the batteries capacity due to their large weight. Moreover, large weight causes instability of flight. Therefore, it is not easy to make the endurance longer, so we must change the point of view.

To improve the efficiency of aerial object transportation within the limited endurance, we focus on a way that aerial robot transports multiple objects at the same time. However, it is difficult for conventional aerial robots to transport multiple objects because multiple grippers are necessary to grasp multiple objects, but when the number of objects the aerial robot grasps changes, the center of gravity(CoG) position of the aerial robot changes, resulting that the flight control becomes unstable. Therefore, to achieve this purpose, we focus on multirotor with two-dimensional multilinks[10] which possesses the ability to modify the CoG position actively. When picking up an object, the multirotor with multilinks can keep the flight control stable by the aerial transformation by which the CoG position can be modified. In previous works[6][7][10], quad-rotor with four-links was proposed and extension of the number of links was difficult due to the hardware structure. Therefore, to extend the number of links, a novel structure of multilinks is necessary.

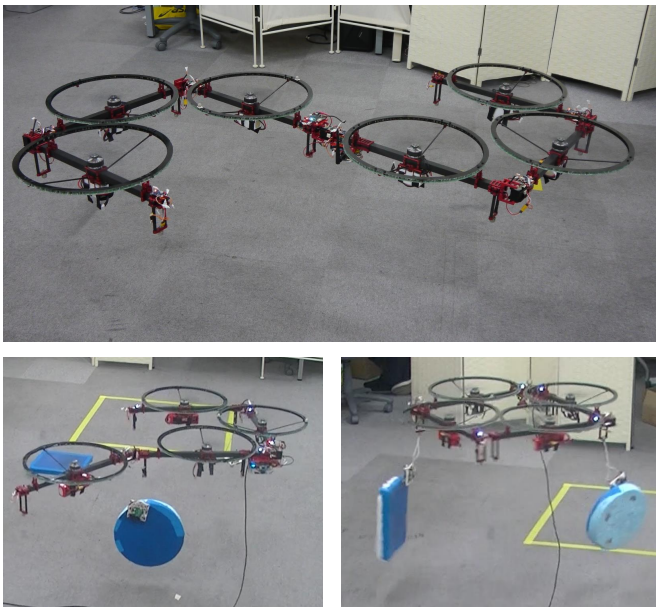

Fig. 1. Upper: the multirotor with multilinks which can transform in the air. Lower left: the aerial robot grasps one object. Lower right: the aerial robot grasps two objects.

The main purpose of this paper is to achieve the construction of the hardware platform of the multirotor with multilinks and multiple objects transportation. Sec. II describes the general approach for the multiple objects transportation. Sec. III clarifies the model of the transformable aerial robot and flight control for aerial transformation. In Sec. IV, we propose the hardware platform which includes the construction of link module and internal communication system. Sec. V explains how to find the optimal form of the multirotor with multilinks based on the flight stability. Finally, we present experimental results in Sec. VI to demonstrate the feasibility of the multiple object transportation by the multirotor with multilinks.

[1]T. Anzai, M. Zhao, X. Chen, F. Shi, K. Kawasaki, K. Okada and M. Inaba are with Department of Mechano-Informatics, The University of Tokyo, 7-3-1 Hongo, Bunkyo-Ku, Tokyo 113-8656, Japan anzai at jsk.t.u-tokyo.ac.jp

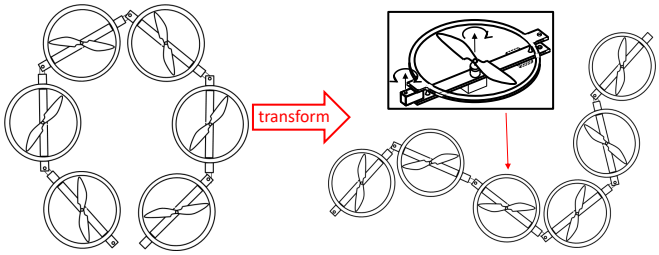

Fig. 2. The structure and transformation of multirotor with multilinks. The multilinks consist of link modules.

II. APPROACHES TO MULTIPLE OBJECT TRANSPORTATION

A. Transformable Multirotor with Two-dimensional Multilink

Zhao et al.[10] proposed a transformable multirotor comprising link modules with built-in propellers and achieved the stable aerial transformation. In other works[6][7], they achieved the aerial manipulation by using the whole body of the transformable aerial robot. The joints with the same rotational axis allows the two-dimensional transformation as shown in Fig. 2. In this work, we focus on the fact that this aerial robot posesses the ability to modify the CoG position actively. Thus, this aerial robot can keep the flight stable by aerial transformation although the number of objects it grasps changes. Therefore, using this way, we approach to the multiple object transportation.

B. Hardware Platform

In previous works [6][7][10], quad-rotor with four-links was proposed and used in experiments. However, extension of the number of links was difficult due to the hardware structure: one central processor is connected to all actuators and sensors. Therefore, to extend the number of links, a novel structure of multilinks is necessary. For this reason, we construct a new link module which can be connected to each other easily. We also develop multi-layer structure for internal communication. Oung et al.[11] proposed multi-propeller platform consisting of single-propeller modules and used infrared transceivers for communication of each single-propeller modules, but it is considered that the communication speed with infrared transceivers is relatively low. Thus, we construct a wired network for communication of each link module.

C. Form Optimization Based on Flight Stability

To keep the flight stable by aerial transformation, the multirotor with multilinks must transform to a particular form. In this work, to obtain the form, we propose the method of form optimization based on flight stability. In Sec. IV, firstly, we investigate the definition of flight stability. Secondly, constraints of form considering the geometric condition and control stability is introduced. Finally, optimal form is obtained by using gradient descent.

III. FLIGHT CONTROL FOR AERIAL TRANSFORMATION

A. Dynamic Model

We assume that the multilinks act as a single rigid body at each time point, since the aerial transformation is operated slowly. With this assumption, the dynamics of the translational motion and rotational motion can be written as follows:

$$M\ddot{\boldsymbol{r}}_{CoG} = \begin{bmatrix} 0 \\ 0 \\ -Mg \end{bmatrix} + R \begin{bmatrix} 0 \\ 0 \\ \sum_{i=1}^{N} F_i \end{bmatrix}; R = R_z(\psi)R_y(\theta)R_x(\varphi) \tag{1}$$

$$I_{multilinks} \begin{bmatrix} \dot{w_x} \\ \dot{w_y} \\ \dot{w_z} \end{bmatrix} = \begin{bmatrix} \sum_{i=1}^{N} y_i F_i \\ -\sum_{i=1}^{N} x_i F_i \\ \sum_{i=1}^{N} T_i \end{bmatrix} - \begin{bmatrix} w_x \\ w_y \\ w_z \end{bmatrix} \times I_{multilinks} \begin{bmatrix} w_x \\ w_y \\ w_z \end{bmatrix} \tag{2}$$

where $\boldsymbol{r}_{CoG}$ and $I_{multilink}$ are the positions of the center of mass and the principal moment of inertia respectively. $[\ w_x\ w_y\ w_z\ ]^{\mathrm{T}}$ is the vector of the angular velocity of the multilinks ,while $[\ \dot{\varphi}\ \dot{\theta}\ \dot{\psi}\ ]^{\mathrm{T}}$ are the time derivatives of Euler angles roll, pitch and yaw respectively.

B. Attitude and Altitude Control Based on LQI Control

As described in previous work[10], the dynamics of the model can be integrated into the simultaneous equations as follows:

$$\ddot{\boldsymbol{y}} = P\boldsymbol{u} - \boldsymbol{G} \tag{3}$$

$$\boldsymbol{y} = [\ z\ \varphi\ \theta\ \psi\ ]^{\mathrm{T}};\ \boldsymbol{u} = [\ F_1\ \cdots\ F_N\ ]^{\mathrm{T}};\ \boldsymbol{G} = [\ g\ 0\ 0\ 0\ ]^{\mathrm{T}}$$

Note that matrix P represents the configuration of the multilinks, including the arrangement of the propellers. It is significant that matrix P is not constant for the transformable multirotor while that is constant for conventional aerial robots.

$$P = [\ \mathbf{p}_z\ \mathbf{p}_x\ \mathbf{p}_y\ \mathbf{p}_c\ ]^{\mathrm{T}} \tag{4}$$

$$\mathbf{p}_z = [\ \bar{m}_1\ \cdots\ \bar{m}_N\ ]^{\mathrm{T}};\ \mathbf{p}_x = [\ \bar{x}_1\ \cdots\ \bar{x}_N\ ]^{\mathrm{T}};$$

$$\mathbf{p}_y = [\ \bar{y}_1\ \cdots\ \bar{y}_N\ ]^{\mathrm{T}};\ \mathbf{p}_c = [\ \bar{c}_1\ \cdots\ \bar{c}_N\ ]^{\mathrm{T}};$$

$$\bar{x}_i = \frac{-x_i}{I_{multi_y y}},\ \bar{y}_i = \frac{y_i}{I_{multi_x x}},\ \bar{c}_i = \frac{c_i}{I_{multi_z z}},\ \bar{m}_i = \frac{1}{M}$$

We introduce the following state equation for linear-quadratic-integral(LQI) system about attitude and altitude control with the new state($\boldsymbol{x} = [\ z\ \dot{z}\ \varphi\ \dot{\varphi}\ \theta\ \dot{\theta}\ \psi\ \dot{\psi}\ ]^{\mathrm{T}}$).

$$\dot{\boldsymbol{x}} = A\boldsymbol{x} + B\boldsymbol{u} + \boldsymbol{d} \tag{5}$$

$$\boldsymbol{y} = C\boldsymbol{x} \tag{6}$$

$$\boldsymbol{x} \in R^8,\ \boldsymbol{u} \in R^N,\ \boldsymbol{y} \in R^4,\ \boldsymbol{d} \in R^8$$

where

$$A = \begin{bmatrix} 0 & 1 & 0 & 0 & 0 & 0 & 0 & 0 \\ 0 & 0 & 0 & 0 & 0 & 0 & 0 & 0 \\ 0 & 0 & 0 & 1 & 0 & 0 & 0 & 0 \\ 0 & 0 & 0 & 0 & 0 & 0 & 0 & 0 \\ 0 & 0 & 0 & 0 & 0 & 1 & 0 & 0 \\ 0 & 0 & 0 & 0 & 0 & 0 & 0 & 0 \\ 0 & 0 & 0 & 0 & 0 & 0 & 0 & 1 \\ 0 & 0 & 0 & 0 & 0 & 0 & 0 & 0 \end{bmatrix}$$

$$B = [\mathbf{0}\ \boldsymbol{p}_z\ \mathbf{0}\ \boldsymbol{p}_x\ \mathbf{0}\ \boldsymbol{p}_y\ \mathbf{0}\ \boldsymbol{p}_c]^{\mathrm{T}}$$

$$C = \begin{bmatrix} 1 & 0 & 0 & 0 & 0 & 0 & 0 & 0 \\ 0 & 0 & 1 & 0 & 0 & 0 & 0 & 0 \\ 0 & 0 & 0 & 0 & 1 & 0 & 0 & 0 \\ 0 & 0 & 0 & 0 & 0 & 0 & 1 & 0 \end{bmatrix}$$

In Eq. 5 $\sim$ Eq. 6, $\boldsymbol{u}$ and $\boldsymbol{y}$ are the input and output of the control system, while $\boldsymbol{d} = [\ 0\ \ -g\ \ 0\ \ 0\ \ 0\ \ 0\ \ 0\ \ 0\ ]^{\mathrm{T}}$ can be regarded as constant noise in the control system.

We extend the state equation by modifying the state and input as follows:

$$\tilde{\boldsymbol{x}} \equiv \boldsymbol{x} - \boldsymbol{x}_s;\ \tilde{\boldsymbol{u}} \equiv \boldsymbol{u} - \boldsymbol{u}_s \tag{7}$$

where $\boldsymbol{x}_s$ and $\boldsymbol{u}_s$ are the final values at the steady state.

We also introduce a tracking error between the reference input and the system output $\boldsymbol{e}$ and the integral value $\boldsymbol{v}$ as follows:

$$\dot{\boldsymbol{v}} = \boldsymbol{e} = \boldsymbol{r} - \boldsymbol{y} = C\boldsymbol{x_s} - C\boldsymbol{x} = -C\tilde{\boldsymbol{x}} \tag{8}$$

Based on the extended state equation(Eq. 9), we design a cost function given by Eq. 10.

$$\dot{\bar{\boldsymbol{x}}} = \bar{A}\bar{\boldsymbol{x}} + \bar{B}\tilde{\boldsymbol{u}} \tag{9}$$

$$\bar{\boldsymbol{x}} = \begin{bmatrix} \tilde{\boldsymbol{x}} \\ \boldsymbol{v} \end{bmatrix};\quad \bar{A} = \begin{bmatrix} A & O_{8,4} \\ -C & O_{4,4} \end{bmatrix};\quad \bar{B} = \begin{bmatrix} B \\ O_{4,N} \end{bmatrix}$$

$$J = \int_0^\infty (\bar{\boldsymbol{x}}^{\mathrm{T}} Q \bar{\boldsymbol{x}} + \tilde{\boldsymbol{u}}^{\mathrm{T}} R \tilde{\boldsymbol{u}}) dt \tag{10}$$

where Q and R are the gain matrices to determine the influence on the convergence characteristics of the control system.

Finally we can retrieve the optimal feedback gain from Eq. 9 and Eq. 10 according to the general LQ theory[12].

C. Position Control in the Horizontal Plane

positions control in the x and y planes use the roll and pitch angles as inputs, and the translational accelerations $\ddot{x}$ and $\ddot{y}$ are a consequence of pitch θ and roll φ tilt. The desired accelerations $\ddot{x}^{des}$ and $\ddot{y}^{des}$ are calculated from a general PID controller described in previous work[13]:

$$\ddot{r}^{des}_{CoG} = k_P(r^{des}_{CoG} - r_{CoG}) + k_I \int (r^{des}_{CoG} - r_{CoG}) d\tau + k_D(\dot{r}^{des}_{CoG} - \dot{r}_{CoG}) \tag{11}$$

where the PID gains(k_P, k_I, k_D) are adjusted to achieve the stable hovering position control.

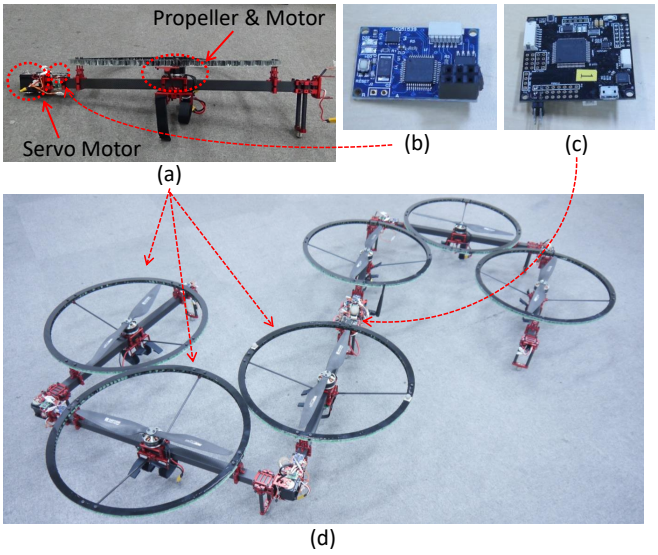

Fig. 3. The hardware components of the multilinked multirotor. (a): the link module of multilinks with built-in propeller at the center, servo motor at the end and controller board(Neuron). (b): controller board Neuron communicating with each device and comprising IMU onboard. (c): controller board Spinal communicating with each Neuron and the onboard computer. (d): transformable hex-rotor with six-links consisting of the link modules.

IV. HARDWARE PLATFORM

A. Structure of Link Module

We constructed the link module of the multilinks as shown in Fig. 3(a). Each link module has a build-in propeller at the center and a servo motor at the end of the link module comprised the main part of the joint module. The rotation range of each joint is $-\frac{\pi}{2}$[rad] $\sim$ $\frac{\pi}{2}$[rad]. The multilinks can transform only in two-dimensions due to the joints with the same rotational axis. The range of lifting force is (0[N]$\sim$16.5[N]). The length of each link is 0.6[m] while the diameter of the propeller protector is 0.38[m].

B. Multi-Layer Structure for Internal Communication

The multirotor with multilinks has not only motors for rotation of propeller but also servo motors for transform as actuator. Besides, the length of the multilinks is longer than conventional aerial robots. In the conventional method, an aerial robot has only one central processor connected to all actuators and sensors. However, it is assumed that if we provide the conventional method for the multilinks, the possibility of disconnection increases due to the length of the multilinks. Matsui et al.[14] made reference to this problem for humanoid robots.

For the reason noted above, we constructed multi-layer structure for internal communication(Fig. 4). As shown in Fig. 3(a), each link module has the controller board(Neuron)(Fig. 3(b)) which sends data to the motor and the servo motor and receives data from IMU(Inertia Measurement Unit). Moreover, the center link has the other controller board(Spinal)(Fig. 3(c)) which communicates with each Neuron. We use CAN(Controller Area Network)[15] to construct the communication system between the controller

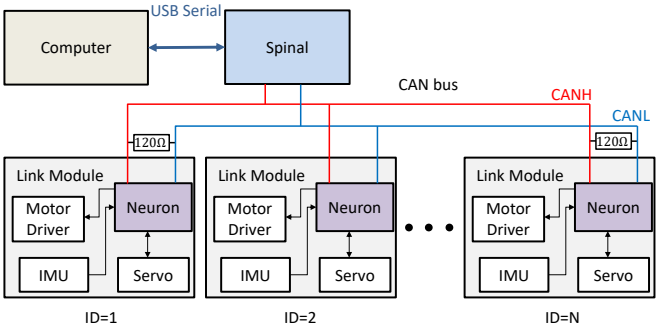

Fig. 4. The multi-layer structure for internal communication comprising Neuron, Spinal and Computer: Neuron communicates with each device(motor, servo motor and IMU) while Spinal communicates with Neuron by using CAN. Computer and Spinal communicate by using USB-Serial.

boards. As used in cars, CAN is a reliable communication system which resists external noise. Thereby, the amount of electric wiring decreases resulting that the reliability of the communication improves.

Moreover, the computer is connected to Spinal on USB-serial communication. The LQI control, motion planning, etc are executed on the computer.

V. FORM OPTIMIZATION BASED ON FLIGHT STABILITY

A. Optimal Form Based on Flight Stability

The dynamics of the model is described is Eq. 4. Therefore, when the control system is at steady state, the control model can be written as follows:

$$P(\boldsymbol{\theta}, m_{obj}, \boldsymbol{r}_{obj})\boldsymbol{u} = \boldsymbol{G} \tag{12}$$

where $\boldsymbol{\theta}$, m_{obj} and $\boldsymbol{r}_{obj}$ denotes the angle vector of joints $(\theta_1, \cdots, \theta_N)$, the mass and the position of a object which the multirotor grasps respectively to emphasize that matrix P is influenced by them.

When any element in $\boldsymbol{u}$ exceeds the range of lifting forces, the flight control is unstable. Although all elements of $\boldsymbol{u}$ fall within the range of forces, any one of them can exceed the range of forces when it is close to the upper limit of forces due to the flight control and disturbance. Hence, the most stable state is that all elements of $\boldsymbol{u}$ are equal since the sum of $\boldsymbol{u}$ equal to MG which is constant at the steady state. This is written as:

$$\mathrm{min} V(\boldsymbol{u}) \text{ subject to } P\boldsymbol{u} = \boldsymbol{G} \tag{13}$$

where the function $V(x)$ is used to calculate the variance of elements of x.

This variance can be written as:

$$V(\boldsymbol{u}) = E(\boldsymbol{u}^2) - E(\boldsymbol{u})^2 \tag{14}$$

where the function $E(x)$ is used to calculate the mean of elements of x.

Note that $E(\boldsymbol{u})^2$ is a constant term since the sum of $\boldsymbol{u}$ is equal to MG at steady state.

Hence, the problem in Eq. 13 can be redefined as:

$$\mathrm{min} \boldsymbol{u}^{\mathrm{T}}\boldsymbol{u} \text{ subject to } P\boldsymbol{u} = \boldsymbol{G} \tag{15}$$

When $N = 4$ and P is full rank, Eq. 12 can be solved as $\boldsymbol{u} = P^{-1}\boldsymbol{G}$. However, for a system with more than four links, a null space occurs, resulting in an infinite solution for $\boldsymbol{u}$. In this case, we use Lagrange multiplier to obtain least-norm solution of $\boldsymbol{u}$ since the purpose is to minimize the norm of $\boldsymbol{u}$ as shown in Eq. 15.

The Lagrange multiplier can be written as:

$$\boldsymbol{u} = P(PP^{\mathrm{T}})^{-1}\boldsymbol{G} \tag{16}$$

B. Constraints of Form of Multilinks

Even though the optimal form can be obtained as described in Eq. 15, the solution can be invalid. Therefore, the solution must satisfy constraints to avoid invalid forms. Five constraints are shown as follows.

1) Joint Angle Limit: In this work, the rotation range of each joint is $-\frac{\pi}{2}$[rad] $\sim$ $\frac{\pi}{2}$[rad]. The joint angles must be changed in this range since a command of joint angle which is out of this range does not make sense.

2) Self-Collision: Although the joint angles are in the range, self-collision can occur as shown in Fig. 5(a). Therefore, collision detection is necessary to avoid self-collision.

3) Rank of P: According to Eq. 4, if P has full rank, the mapping is surjective, indicating that the four elements in $\boldsymbol{y}$ $(z, \varphi, \theta, \psi)$ are dependent of each other. In contrast, if P is not of full rank, the four elements can not act independently, leading to an uncontrollable result. We call the resulting special form the singular form(Fig. 5(b)).The rank of P can be calculated by checking the linear combination of row vectors $(\mathbf{p}_z, \mathbf{p}_x, \mathbf{p}_y, \mathbf{p}_c)$. When the multirotor is under the singular form, its control system is asymptotically unstable.

4) Lifting Force Range: Lifting force which is generated by the propeller has the range. In the case of our own machine, the range of lifting force is (0[N]$\sim$16.5[N]). All elements of the input vector $\boldsymbol{u}$ in Eq. 16 must fall within this range of forces.

5) Distance from Each Propeller to the Rotational Axis: There can be unavoidable errors in the control model(Eq. 4) and state equation(Eq. 5) because of estimation errors in the inertia parameters. The most serious error concerns the estimation of x_i and y_i as shown in Fig. 6. The distance x_i, y_i has a significant effect on the moment for pitch and roll rotation, especially when all elements in x or y are close to zero, in which case the estimation error can assign the wrong sign of x_i, y_i, producing a roll/pitch moment in the wrong direction.

To avoid this, it is necessary to keep the distance x_i, y_i large enough. We, therefore, introduce the following distance indices d_x, d_y to evaluate each state:

$$\begin{cases} d_x(State(\boldsymbol{\theta})) = \frac{\min(|\min(\boldsymbol{x}(\boldsymbol{\theta}))|, \max(\boldsymbol{x}(\boldsymbol{\theta})))}{r} \\ d_y(State(\boldsymbol{\theta})) = \frac{\min(|\min(\boldsymbol{y}(\boldsymbol{\theta}))|, \max(\boldsymbol{y}(\boldsymbol{\theta})))}{r} \end{cases} \tag{17}$$

We then use the indices to validate the state in terms of the distance of pitch/roll moment, using a thresholding method

as follows:

$$Validator_{dist}(State(\boldsymbol{\theta})) =$$
$$\begin{cases} Valid & (d_x(State(\boldsymbol{\theta})) >= Threshold \\ & AND\ d_y(State(\boldsymbol{\theta})) >= Threshold) \\ Invalid & (d_x(State(\boldsymbol{\theta})) < Threshold \\ & OR\ d_y(State(\boldsymbol{\theta})) < Threshold) \end{cases} \quad (18)$$

The target state will be validated as an invalid state, if either of the two indices fall below the threshold. The form shown in Fig. 5(c) is an example of an invalid state.

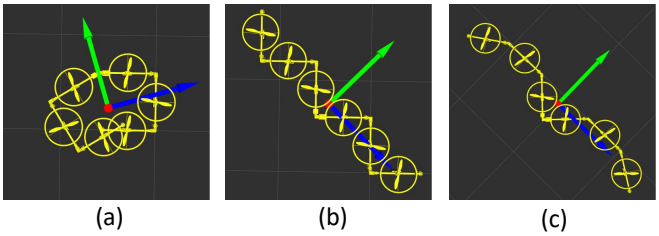

Fig. 5. Examples of invalid forms.
(a): Self-collision form($\theta_1 = \theta_2 = \theta_4 = \theta_5 = \frac{\pi}{2}$[rad], $\theta_3 = 0.55$[rad]).
(b): Singular form($\theta_1 = \theta_3 = \theta_5 = \frac{\pi}{2}$[rad], $\theta_2 = \theta_4 = -\frac{\pi}{2}$[rad]).
(c): Invalid form based on roll/pitch moment($\theta_1 = \theta_5 = 0.80$[rad], $\theta_2 = \theta_4 = 0.57$[rad], $\theta_3 = -\frac{\pi}{2}$[rad]).

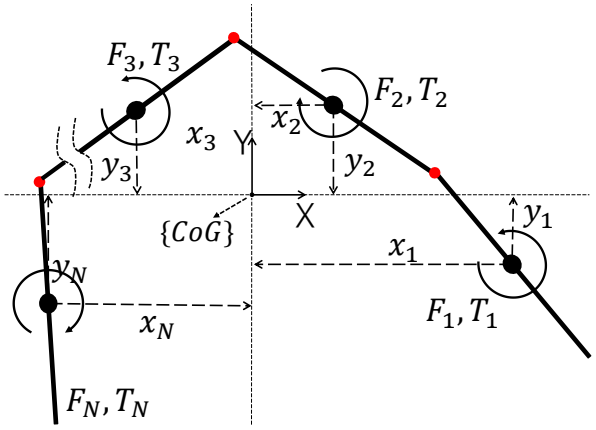

Fig. 6. The dynamic model of the quadrotor prototype described in coordinate frame $\{CoG\}$. F_i and T_i denote the lifting force and torque generated by each propeller, respectively. $[x_i, y_i]$ is the location of each propeller in the frame of $\{CoG\}$.

C. Optimal Form Based on Gradient Descent

To determine the joint angle vector $\boldsymbol{\theta}$ which minimizes $\boldsymbol{u}^{\mathrm{T}}\boldsymbol{u}$(Eq. 15, Eq. 16), we apply gradient descent(steepest descent)[16]. In gradient descent, the joint angle vector $\boldsymbol{\theta}$ is updated as follows:

$$\boldsymbol{\theta}^{(k+1)} = \boldsymbol{\theta}^{(k)} - \alpha\ \mathrm{grad}(F(\boldsymbol{\theta}^{(k)})) \quad (19)$$
$$F(\boldsymbol{\theta}) = \boldsymbol{u}(\boldsymbol{\theta})^{\mathrm{T}}\boldsymbol{u}(\boldsymbol{\theta})$$

Note that α is a parameter which determines the weight of one update and is normally defined as small positive value. Although F is necessary to be differentiable, it is a simple method since only first derivative must be calculated. In this work, as it is difficult to calculate partial derivative of F, instead of this, we calculate variation of F. This is written as:

$$\mathrm{grad}(F(\boldsymbol{\theta}))_i = \frac{F(\boldsymbol{\theta} + \Delta\boldsymbol{\theta_i}) - F(\boldsymbol{\theta})}{\Delta\theta} \quad (20)$$

where $\Delta\theta$ and $\Delta\boldsymbol{\theta_i}$ are infinitesimal angle and column vector whose i-th component is $\Delta\theta$ and the other components are 0, respectively. We also introduce V_{th}, the lower limit of $V(\boldsymbol{u})$ as a termination condition of optimization. Since the upper limit of lifting force is 16.5[N] in the case of our own machine, we set V_{th} to 0.001[N^2]. In other words, we stop the optimization when $V(\boldsymbol{u})$ is 0.001[N^2] since the value can be considered to be converged fully. Besides, since the solution obtained by gradient descent depends on the initial value, there is a possibility that valid solution is not obtained. Accordingly, we perform optimization with multiple initial values($\theta_i = 0.0, 0.1, \cdots, 1.0$).

Then, setting parameters of gradient descent as shown in Table I, we perform optimization calculation on four conditions shown in Fig. 7. In Fig. 7(a) $\sim$ Fig. 7(d), the orange circle indicates the position of the additional mass(0.5[kg]) while the red circle and the blue, green arrows indicate the position of CoG and principal axes of inertia, respectively. According to the final values of $V(\boldsymbol{u})$ shown under each form, it is evident that the optimization is fully performed and optimal forms can be obtained by this method.

TABLE I
PARAMETERS OF GRADIENT DESCENT.

parameter	value	description
α	0.3	weight of update[rad^2/N^2]
m_{UAV}	5	UAV mass[kg]
m_{obj}	0.5	additional mass[kg]
V_{th}	0.001	lower limit of $V(\boldsymbol{u})$[N^2]

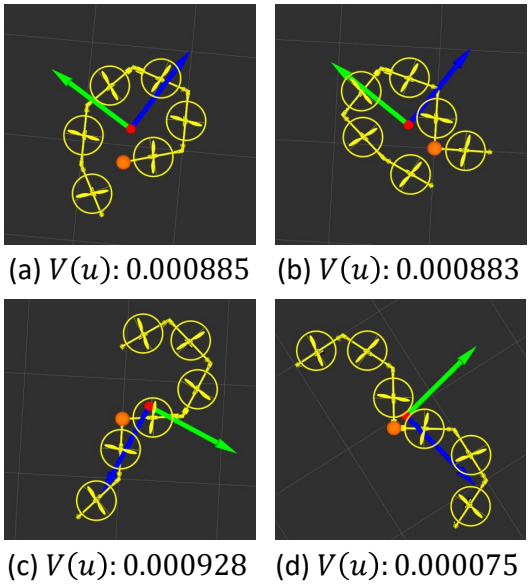

Fig. 7. The optimized forms of each case with gradient descent: the values under each form is the final value of $V(\boldsymbol{u})$.

VI. EXPERIMENTS

A. Aerial Transformation

In this section, we utilize a transformable quad-rotor with four-links. The whole weight is about 3.3[kg]. The three-dimensional position was tracked by a motion capture system, representing nearly ground truth, and sent to the onboard computer via Wi-Fi. The hardware and software system is the same as that explained in Sec. V.

We test the stability of hovering of multilinks under a fixed form($\theta_1 = \theta_2 = \frac{\pi}{2}$, $\theta_3 = 0$, $\theta_4 = \theta_5 = -\frac{\pi}{2}$) and the result is shown in Fig. 8. In Fig. 8(a), each element of lifting force disperses after about 10[s], resulting that u_3(the third element of lifting force $\boldsymbol{u}$) reaches the upper limit(16.5[N]). The reason can be explained by the result shown in Fig. 8(b). After about 10[s], the error of yaw angle increases, and then a particular lifting force increases due to the feedback control of yaw angle. Normally, the error of yaw angle converges to the target angle which is 0 in this experiment by the attitude control, however. Therefore, it is assumed that there are some factors which is not considered in the control model. As one of the factors, tilt of propeller axis resulting from the low rigidity of multilinks can be considered. If an propeller axis tilts, the moment around yaw axis is generated. The moment can be regarded as a disturbance which affects yaw angle. The moment generated by a propeller scales linearly with the lifting force generated by the propeller. This is written as:

$$T_i = c_i F_i \ (i = 1, \cdots, N) \tag{21}$$

$$c_i = \pm 0.01676 \tag{22}$$

where T_i and F_i indicate the moment and lifting force generated by i-th propeller, respectively. Also note that c_i is a constant rate between moment and force. The sign of c_i is positive when the propeller rotates CCW and negative when the propeller rotates CW. In our multilinks, the value of c_i is shown in Eq. 22. That is to say, since the disturbance moment generated by tilt of the propeller is larger than the propeller moment(T_i), resulting in divergence of the input vector $\boldsymbol{u}$.

Assuming this, we also performed a experiment on aerial transformation by hex-rotor with six-links with the following start and goal forms:

$$\begin{cases} START : \theta_i = \frac{\pi}{3}[\text{rad}] \\ GOAL : \theta_i = -\frac{\pi}{3}[\text{rad}] \end{cases} \tag{23}$$

Fig. 9 shows the snapshots of the aerial transformation, while Fig. 10 shows the result of change of joint angle, yaw angle and three-dimensional position.

B. Multiple Objects Transportation

In this work, limiting target objects to ferrous objects, we construct an electromagnet gripper. The gripper comprises five electromagnets whose diameter is 20[mm] and four micro switches. Contact with an object can be detected by the signal of micro switches. The electromagnets are driven only while any switch is turned on to save the energy of batteries and to avoid the overheating of electromagnets. The gripper communicates with a computer by using USB-Serial.

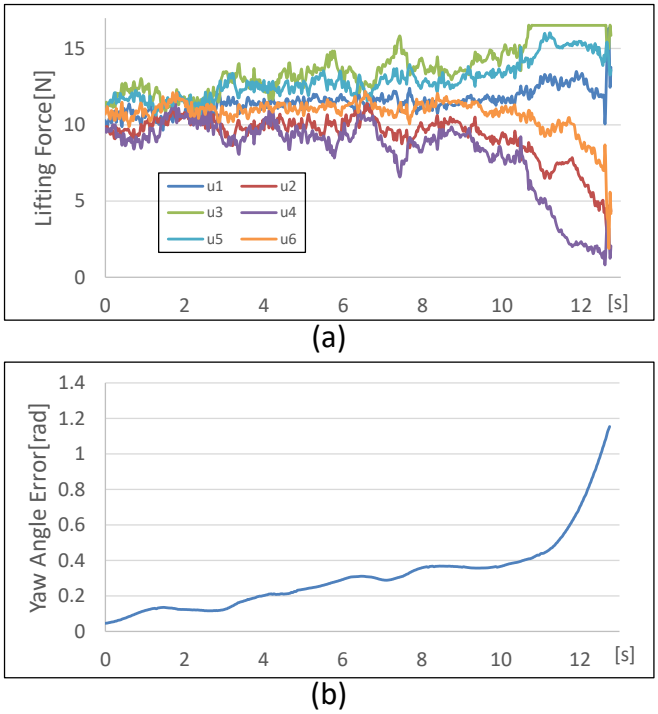

Fig. 8. Experimental result of hovering with yaw control. (a): Change of lifting force generated by each propeller. (b): Change of yaw angle.

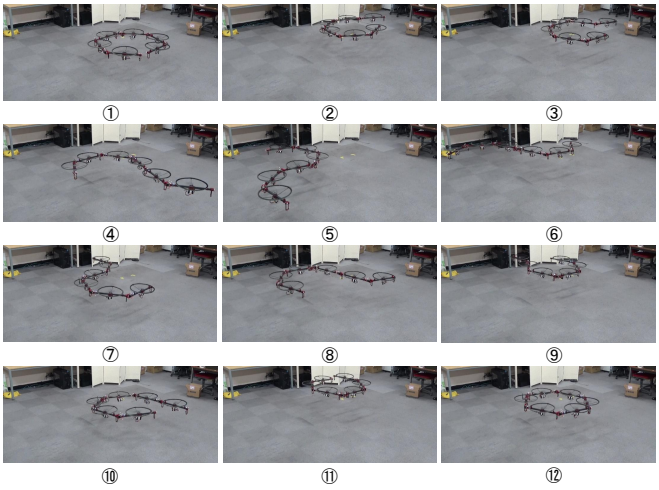

Fig. 9. Experiment of aerial transformation by six-links without yaw control: the start form is ($\theta_i = \frac{\pi}{3}$) and the goal form is ($\theta_i = -\frac{\pi}{3}$).

The number of target objects was set to 2. Then, using the form optimization method, we calculated optimal forms shown in Fig. 11. The additional mass is 0.551[kg], the sum weight of the target object and the electromagnet gripper. The final values of $V(\boldsymbol{u})$ shown under each form, especially that of form (b), are large relatively. The cause is considered that the four-links lacks the degree of freedom of transform due to the constraints described in Sec. V(b).

Then, we performed the experiment of multiple object transportation as shown in Fig. 12. The process of multiple object transportation can be summarized as follows: ①: approaching to the first object; ② $\sim$ ④: grasping the first object and transforming to the optimal form(Fig. 11(b)); ⑤: approaching to the second object; ⑥ $\sim$ ⑧: grasping the second object and transforming to the optimal form(Fig. 11(c)); ⑨ $\sim$ ⑩: approaching to and landing on the goal area. The positions of the objects were detected by a camera on the aerial robot with using HSV-Filter to detect the blue region. Note that the optimal forms were calculated in off-line in this work since the weight of the objects were given in advance.

VII. CONCLUSIONS

In this paper, we proposed a methodology of multiple objects transportation by the transformable multirotor with two-dimensional multilinks. We then described the form optimization method to obtain the optimal form based on the flight stability, along with the definition of the flight stability and constraints of forms to avoid invalid forms. We then developed the hardware and software system, including the multi-layer structure for internal communication. Finally, we showed the effectiveness of the proposed method by an experiment. In the experiment, we show the achievement of aerial transformation and multiple objects transportation.

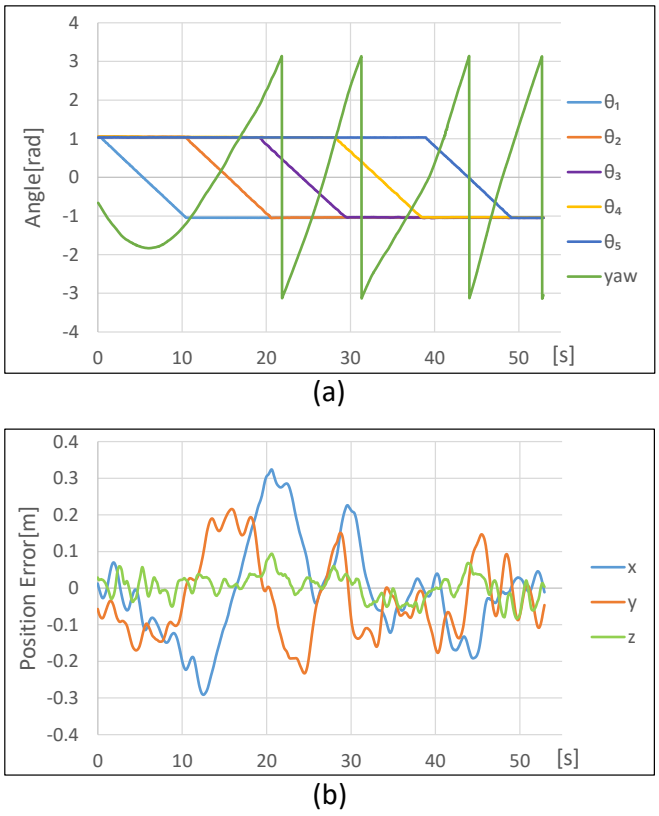

Fig. 10. (a): Change of angle of each joint and yaw angle. (b): Change of three-dimensional position error.

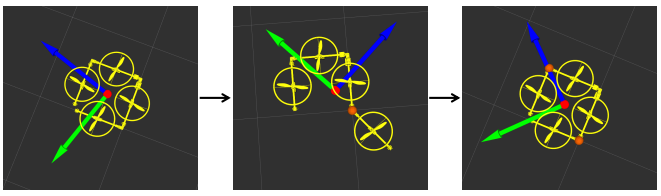

Fig. 11. The optimal forms of quad-rotor with four-links: the aerial robot grasps (a):no object (b): one object (c): two objects

For future work, we will construct more rigid link module to achieve the aerial transformation with yaw control. Next, while the optimal form was calculated in off-line in this work, we will calculate that in on-line by estimating the weight of target objects based on change of the lifting force. Then, we must accelerate the calculation of the form optimization. Moreover, we are interested in multiple objects transportation by using whole-body aerial manipulation[7], in which it is appeared that eight or more links are necessary.

REFERENCES

[1] Vijay Kumar and Nathan Michael. Opportunities and challenges with autonomous micro aerial vehicles. *The International Journal of Robotics Research*, Vol. 31, No. 11, pp. 1279–1291, 2012.

[2] Lefteris Doitsidis, Stephan Weiss, Alessandro Renzaglia, Markus W. Achtelik, Elias Kosmatopoulos, Roland Siegwart, and Davide Scaramuzza. Optimal surveillance coverage for teams of micro aerial ve-

hicles in gps-denied environments using onboard vision. *Autonomous Robots*, Vol. 33, No. 1, pp. 173–188, 2012.

[3] Markus Bernard, Konstantin Kondak, Ivan Maza, and Anibal Ollero. Autonomous transportation and deployment with aerial robots for search and rescue missions. *Journal of Field Robotics*, Vol. 28, No. 6, pp. 914–931, 2011.

[4] Quentin Lindsey, Daniel Mellinger, and Vijay Kumar. Construction with quadrotor teams. *Autonomous Robots*, Vol. 33, No. 3, pp. 323–336, 2012.

[5] D. Mellinger, Q. Lindsey, M. Shomin, and V. Kumar. Design, modeling, estimation and control for aerial grasping and manipulation. In *2011 IEEE/RSJ International Conference on Intelligent Robots and Systems*, pp. 2668–2673, 2011.

[6] *Transformable Multirotor with Two-dimensional Multilinks: Modeling, Control, and Whole-body Aerial Manipulation*, 2016.

[7] *Whole-body Aerial Manipulation by Transformable Multirotor with Two-dimensional Multilinks*, 2017.

[8] M. Bernard and K. Kondak. Generic slung load transportation system using small size helicopters. In *2009 IEEE International Conference on Robotics and Automation*, pp. 3258–3264, 2009.

[9] Hugh Durrant-Whyte, Nicholas Roy, and Pieter Abbeel. *Construction of Cubic Structures with Quadrotor Teams*, pp. 177–184. MIT Press, 2012.

[10] Moju Zhao, Koji Kawasaki, Kei Okada, and Masayuki Inaba. Transformable multirotor with two-dimensional multilinks: modeling, control, and motion planning for aerial transformation. *Advanced Robotics*, Vol. 30, No. 13, pp. 825–845, 2016.

[11] R. Oung, F. Bourgault, M. Donovan, and R. D'Andrea. The distributed flight array. In *Robotics and Automation (ICRA), 2010 IEEE International Conference on*, pp. 601–607, 2010.

[12] P. C. YOUNG and J. C. WILLEMS. An approach to the linear multivariable servomechanism problem †. *International Journal of Control*, Vol. 15, No. 5, pp. 961–979, 1972.

[13] Moju Zhao, Koji Kawasaki, Yohei Kakiuchi, Kei Okada, and Masayuki Inaba. Simultaneous environment modeling and deployment of network by dropping wireless modules based on radio field intensity measurement using an micro aerial robot. *Journal of the Robotics Society of Japan*, Vol. 32, No. 7, pp. 643–650, 2014.

[14] T. Matsui, H. Hirukawa, Y. Ishikawa, N. Yamasaki, S. Kagami, F. Kanehiro, H. Saito, and T. Inamura. Distributed real-time processing for humanoid robots. In *11th IEEE International Conference on Embedded and Real-Time Computing Systems and Applications (RTCSA'05)*, pp. 205–210, 2005.

[15] K. Etschberger. *Controller Area Network: Basics, Protocols, Chips and Applications*. 2001.

[16] Takashi OZEKI. A convergent property of steepest descent method in minimizing nonlinear functions. *IEICE technical report. Nonlinear problems*, Vol. 103, No. 375, pp. 13–18, oct 2003.

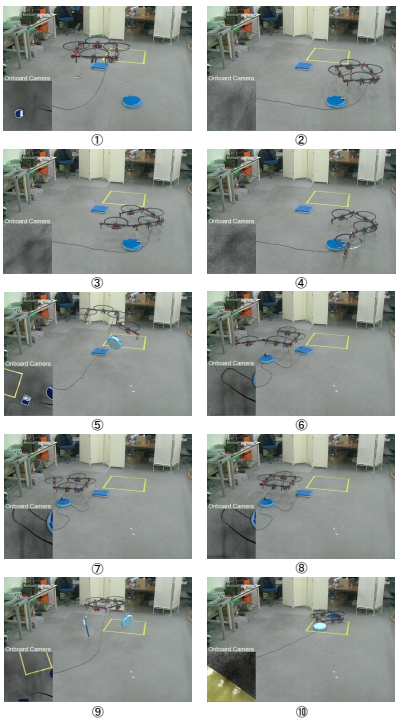

Fig. 12. Experiment of multiple objects transportation: two ferrous objects are grasped and transpo rted by the transformable aerial robot.